

Magnetic moments of the spin-1/2 singly charmed baryons in covariant baryon chiral perturbation theory

Rui-Xiang Shi,¹ Yang Xiao,¹ and Li-Sheng Geng^{1,*}

¹*School of Physics and Nuclear Energy Engineering & International Research Center for Nuclei and Particles in the Cosmos & Beijing Key Laboratory of Advanced Nuclear Materials and Physics, Beihang University, Beijing 100191, China*

Abstract

Recent experimental advances have reignited theoretical interests in heavy-flavor hadrons. In this work, we study the magnetic moments of the spin-1/2 singly charmed baryons up to the next-to-leading order in covariant baryon chiral perturbation theory with the extended-on-mass-shell renormalization scheme. The pertinent low energy constants g_{1-4} are fixed with the help of the quark model and the heavy quark spin flavor symmetry, while the remaining d_2 , d_3 , d_5 and d_6 are determined by fitting to the lattice QCD pion-mass dependent data. We study the magnetic moments as a function of m_π^2 and compare our results with those obtained in the heavy baryon chiral perturbation theory. We find that the loop corrections induced by the anti-triplet states are dominated by the baryon pole diagram. In addition, we predict the magnetic moments of the spin-1/2 singly charmed baryons and compare them with those of other approaches.

PACS numbers:

*E-mail: lisheng.geng@buaa.edu.cn

I. INTRODUCTION

In the last two decades, tremendous progress has been made in our understanding of heavy-flavor hadrons, thanks to the experimental discoveries by collaborations such as LHCb, BELLE, and BESIII and the related theoretical studies. In the charmed baryon sector, 24 singly charmed baryons and two doubly charmed baryons are listed in the current version of the review of particle physics [1]. Among them, the newest members include the $\Lambda_c(2860)$ [2], the five Ω_c states [3], and the Ξ_{cc}^{++} [4]. Inspired by these and other experimental discoveries, there are extensive theoretical and lattice QCD studies on their nature and their decay and production mechanisms (see, e.g., Refs. [5–12] references cited therein).

The magnetic moment of a baryon plays an extremely important role in understanding its internal structure. Historically, the experimental measurement of the magnetic moments of the proton and the neutron revealed that they are not point-like particles. The subsequent studies helped the establishment of the quark model as well the theory of the strong interaction, Quantum Chromo Dynamics. Unlike those of the ground-state baryons, the magnetic moments of the spin-1/2 singly charmed baryons have not been measured experimentally. Nevertheless, they have been studied in a variety of phenomenological models [13–19] as well as QCD sum rules [20]. Lately, they have also been studied in the mean-field approach [21], the self-consistent SU(3) chiral quark-soliton model [22], the heavy baryon chiral perturbation theory (HB ChPT) [23], and lattice QCD simulations [24–27]. In Ref. [23], the low energy constants (LECs) are determined by the quark model and the heavy quark spin flavor symmetry and by fitting to the lattice QCD data extrapolated to the physical point. In this work, we will study the magnetic moments of the spin-1/2 singly charmed baryons up to the next-to-leading order (NLO) in covariant baryon chiral perturbation theory (BChPT) with the extended-on-mass shell (EOMS) renormalization scheme. The unknown LECs will be determined by the quark model and the heavy quark spin flavor symmetry and by directly fitting to the lattice QCD data at unphysical pion masses [24–26]. One notes that many previous studies, such as Refs. [28, 29], have shown that the EOMS BChPT can provide a better description of the lattice QCD quark-mass dependent data than its non-relativistic counterpart.

Chiral perturbation theory (ChPT) [30], as a low-energy effective field theory of QCD, is an appropriate framework to study the magnetic moments of hadrons, particularly, their light quark mass dependence. It provides a systematic expansion of physical observables in powers of $(p/\Lambda_\chi)^{n_\chi}$, where p is a small momentum and Λ_χ is the chiral symmetry breaking scale. However, its application to the one-baryon sector encountered a difficulty, i.e., a systematic power counting (PC) is lost due to the large non-vanishing baryon mass m_0 in the chiral limit. Over the years, three approaches were proposed to overcome this issue, i.e., the HB [31, 32], the infrared (IR) [33], and the EOMS [34] schemes. The IR and the EOMS schemes are the

relativistic formulations of BChPT. A brief summary and comparison of the three different approaches can be found in Ref. [35].

The EOMS scheme is different from the HBChPT, because it retains a series of higher-order terms within the covariant power counting (PC) rule when removing the power-counting-breaking (PCB) terms. In recent years, many physical observables have been successfully studied in this scheme such as the magnetic moments [29, 36–40], the masses and sigma terms [28, 41–43] of the octet, decuplet and spin-1/2 doubly heavy baryons, the hyperon vector couplings [44, 45], the axial vector charges [46], the pion nucleon [47, 48] and kaon-nucleon scattering [49]. Thus, inspired by these studies, we would like to study the magnetic moments of the spin-1/2 singly charmed baryons in the EOMS scheme.

This work is organized as follows. In Sec. II, we provide the effective Lagrangians and calculate the relevant Feynman diagrams up to $O(p^3)$. Results and discussions are given in Sec. III, followed by a short summary in Sec. IV.

II. THEORETICAL FORMALISM

The magnetic moments of singly charmed baryons are defined via the matrix elements of the electromagnetic current J_μ as follows:

$$\langle \psi(p_f) | J_\mu | \psi(p_i) \rangle = \bar{u}(p_f) \left[\gamma_\mu F_1^B(q^2) + \frac{i\sigma_{\mu\nu}q^\nu}{2m_B} F_2^B(q^2) \right] u(p_i),$$

where $\bar{u}(p_f)$ and $u(p_i)$ are the Dirac spinors, m_B is the singly charmed baryon mass, and $F_1^B(q^2)$ and $F_2^B(q^2)$ denote the Dirac and Pauli form factors, respectively. The four-momentum transfer is defined as $q = p_i - p_f$. At $q^2 = 0$, $F_2^B(0)$ is the so-called anomalous magnetic moment, κ_B , and the magnetic moment is $\mu_B = \kappa_B + Q_B$, where Q_B is the charge of the singly charmed baryon.

The five Feynman diagrams contributing to μ_B up to $O(p^3)$ are shown in Fig.1. The leading order contribution of $O(p^2)$ is provided by the following Lagrangian:

$$\begin{aligned} \mathcal{L}_{33}^{(2)} &= \frac{d_2}{16m_{\bar{3}}} \text{Tr}(\bar{B}_{\bar{3}} \sigma^{\mu\nu} F_{\mu\nu}^+ B_{\bar{3}}) \\ &\quad + \frac{d_3}{16m_{\bar{3}}} \text{Tr}(\bar{B}_{\bar{3}} \sigma^{\mu\nu} B_{\bar{3}}) \text{Tr}(F_{\mu\nu}^+), \\ \mathcal{L}_{66}^{(2)} &= \frac{d_5}{8m_6} \text{Tr}(\bar{B}_6 \sigma^{\mu\nu} F_{\mu\nu}^+ B_6) \\ &\quad + \frac{d_6}{8m_6} \text{Tr}(\bar{B}_6 \sigma^{\mu\nu} B_6) \text{Tr}(F_{\mu\nu}^+), \end{aligned} \tag{1}$$

where the numbers in the superscript are the chiral order, $\sigma^{\mu\nu} = \frac{i}{2}[\gamma^\mu, \gamma^\nu]$, $F_{\mu\nu}^+ = |e|(u^\dagger Q_h F_{\mu\nu} u + u Q_h F_{\mu\nu} u^\dagger)$, $F_{\mu\nu} = \partial_\mu A_\nu - \partial_\nu A_\mu$, and $Q_h = \text{diag}(1, 0, 0)$ is the charge operator of the charmed baryon, $u = \exp[i\Phi/2F_\phi]$,

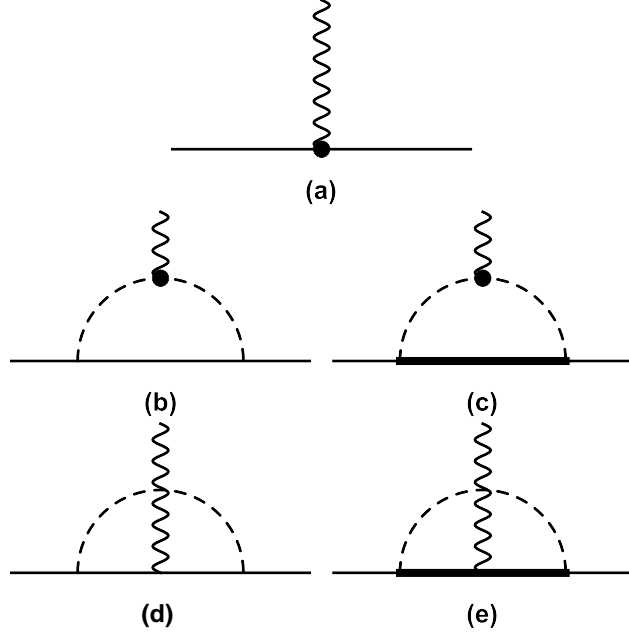


FIG. 1: Feynman diagrams contributing to the singly charmed baryon magnetic moments up to NLO. Diagram (a) contributes at LO, while the other diagrams contribute at NLO. The solid, dashed, and wiggly lines represent singly charmed baryon, Goldstone bosons, and photons, respectively. The heavy dots denote the $\mathcal{O}(p^2)$ vertices.

with the unimodular matrix containing the pseudoscalar nonet, and F_ϕ the pseudoscalar decay constant. In the following analysis, we take $F_\pi = 92.4$ MeV, $F_K = 1.22F_\pi$, and $F_\eta = 1.3F_\pi$. In the SU(3) flavor representation, there are three kinds of singly charmed baryons, which are denoted as $B_{\bar{3}}$, B_6 , and $B_6^{*\mu}$, respectively,

$$B_{\bar{3}} = \begin{pmatrix} 0 & \Lambda_c^+ & \Xi_c^+ \\ -\Lambda_c^+ & 0 & \Xi_c^0 \\ -\Xi_c^+ & -\Xi_c^0 & 0 \end{pmatrix},$$

$$B_6 = \begin{pmatrix} \Sigma_c^{++} & \frac{\Sigma_c^+}{\sqrt{2}} & \frac{\Xi_c'^+}{\sqrt{2}} \\ \frac{\Sigma_c^+}{\sqrt{2}} & \Sigma_c^0 & \frac{\Xi_c'^0}{\sqrt{2}} \\ \frac{\Xi_c'^+}{\sqrt{2}} & \frac{\Xi_c'^0}{\sqrt{2}} & \Omega_c^0 \end{pmatrix}, \quad B_6^{*\mu} = \begin{pmatrix} \Sigma_c^{*++} & \frac{\Sigma_c^{*+}}{\sqrt{2}} & \frac{\Xi_c^{*+}}{\sqrt{2}} \\ \frac{\Sigma_c^{*+}}{\sqrt{2}} & \Sigma_c^{*0} & \frac{\Xi_c^{*0}}{\sqrt{2}} \\ \frac{\Xi_c^{*+}}{\sqrt{2}} & \frac{\Xi_c^{*0}}{\sqrt{2}} & \Omega_c^{*0} \end{pmatrix}. \quad (2)$$

The spin of the $B_{\bar{3}}$ and B_6 states is 1/2 while the spin of the $B_6^{*\mu}$ states is 3/2.

In the numerical analysis, we take the average of the masses for each flavor multiplet, i.e., $m_{\bar{3}} = 2408$ MeV, $m_6 = 2535$ MeV, and $m_{6^*} = 2602$ MeV [1]. The mass differences are $\delta_1 = m_6 - m_{\bar{3}} = 127$ MeV, $\delta_2 = m_{6^*} - m_{\bar{3}} = 194$ MeV, and $\delta_3 = m_{6^*} - m_6 = 67$ MeV.

The loop diagrams arising at NLO are determined in terms of the lowest order LECs from

$\mathcal{L}_B^{(1)} + \mathcal{L}_{MB}^{(1)} + \mathcal{L}_M^{(2)}$, which are,

$$\begin{aligned}
\mathcal{L}_B^{(1)} &= \frac{1}{2}\text{Tr}[\bar{B}_{\bar{3}}(iD - m_{\bar{3}})B_{\bar{3}}] + \text{Tr}[\bar{B}_6(iD - m_6)B_6] \\
&\quad + \text{Tr}[\bar{B}_6^{*\mu}(-g_{\mu\nu}(iD - m_{6^*}) + i(\gamma_\mu D_\nu + \gamma_\nu D_\mu) \\
&\quad - \gamma_\mu(iD + m_{6^*})\gamma_\nu B_6^{*\nu}], \\
\mathcal{L}_{MB}^{(1)} &= \frac{g_1}{2}\text{Tr}[\bar{B}_6\gamma_5 B_6] + \frac{g_2}{2}\text{Tr}[\bar{B}_6\gamma_5 B_{\bar{3}} + \text{h.c.}] \\
&\quad + \frac{g_3}{2}\text{Tr}[\bar{B}_6^{*\mu}u_\mu B_6 + \text{h.c.}] + \frac{g_4}{2}\text{Tr}[\bar{B}_6^{*\mu}u_\mu B_{\bar{3}} + \text{h.c.}] \\
&\quad + \frac{g_5}{2}\text{Tr}[\bar{B}_6^{*\mu}\gamma_5 B_{6\mu}^*] + \frac{g_6}{2}\text{Tr}[\bar{B}_{\bar{3}}\gamma_5 B_{\bar{3}}], \\
\mathcal{L}_M^{(2)} &= \frac{F_\phi^2}{4}\text{Tr}[\nabla_\mu U(\nabla^\mu U)^\dagger], \tag{3}
\end{aligned}$$

with

$$\begin{aligned}
D_\mu B &= \partial_\mu B + \Gamma_\mu B + B\Gamma_\mu^T, \\
\Gamma_\mu &= \frac{1}{2}(u^\dagger\partial_\mu u + u\partial_\mu u^\dagger) - \frac{i}{2}(u^\dagger v_\mu u + u v_\mu u^\dagger) = -ieQ_h A_\mu, \\
u_\mu &= i(u^\dagger\partial_\mu u - u\partial_\mu u^\dagger) + (u^\dagger v_\mu u - u v_\mu u^\dagger), \\
U &= u^2 = e^{\frac{i\phi}{F_\phi}}, \quad \nabla_\mu U = \partial_\mu U + ieA_\mu [Q_l, U], \tag{4}
\end{aligned}$$

where v_μ stands for the vector source, and the charge matrix for the light quark is $Q_l = \text{diag}(2/3, -1/3, -1/3)$.

The total spin of the light quarks is 0 for the singly charmed baryon in the $B_{\bar{3}}$ state. Considering parity and angular momentum conservation, the $B_{\bar{3}}B_{\bar{3}}\phi$ vertex is forbidden, i.e., $g_6 = 0$.

For the $B_{\bar{3}}$ and B_6 states, the tree level contributions of the magnetic moments can be easily obtained from Eq. (1), which are:

$$\begin{aligned}
\kappa_{\bar{3}}^{(a,2)} &= \alpha_{\bar{3}}d_2 + \beta_{\bar{3}}d_3, \\
\kappa_6^{(a,2)} &= \alpha_6d_5 + \beta_6d_6. \tag{5}
\end{aligned}$$

The values of $\alpha_{\bar{3}}, \beta_{\bar{3}}, \alpha_6$, and β_6 are tabulated in Table I and Table II. The four LECs d_2, d_3, d_5 and d_6 will be determined by fitting to lattice QCD data.

At $\mathcal{O}(p^3)$, the loop contributions to the magnetic moments, which come from diagrams (b), (c), (d), and

TABLE I: Coefficients of the tree level contributions of Eq. (5) for the $B_{\bar{3}}$ states.

	Λ_c^+	Ξ_c^+	Ξ_c^0
$\alpha_{\bar{3}}$	$\frac{1}{2}$	$\frac{1}{2}$	0
$\beta_{\bar{3}}$	1	1	1

(e) in Fig. 1, are written as,

$$\begin{aligned}
 \kappa_{\bar{3}}^{(3)} &= \frac{1}{4\pi^2} \left(\sum_{\phi=\pi,K} \frac{g_2^2}{F_\phi^2} \xi_{B_{\bar{3}}\phi,\delta_1}^{(3,b)} H_{B_{\bar{3}}}^{(b)}(\delta_1, m_\phi) \right. \\
 &\quad + \sum_{\phi=\pi,K} \frac{g_4^2}{F_\phi^2} \xi_{B_{\bar{3}}\phi,\delta_2}^{(3,c)} H_{B_{\bar{3}}}^{(c)}(\delta_2, m_\phi) \\
 &\quad + \sum_{\phi=\pi,K,\eta} \frac{g_2^2}{F_\phi^2} \xi_{B_{\bar{3}}\phi,\delta_1}^{(3,d)} H_{B_{\bar{3}}}^{(d)}(\delta_1, m_\phi) \\
 &\quad \left. + \sum_{\phi=\pi,K,\eta} \frac{g_4^2}{F_\phi^2} \xi_{B_{\bar{3}}\phi,\delta_2}^{(3,e)} H_{B_{\bar{3}}}^{(e)}(\delta_2, m_\phi) \right), \\
 \kappa_6^{(3)} &= \frac{1}{4\pi^2} \left(\sum_{\phi=\pi,K} \frac{g_1^2}{F_\phi^2} \xi_{B_6\phi,\delta_1}^{(3,b)} H_{B_6}^{(b)}(0, m_\phi) \right. \\
 &\quad + \sum_{\phi=\pi,K} \frac{g_2^2}{F_\phi^2} \xi_{B_6\phi,\delta_1}^{(3,b)} H_{B_6}^{(b)}(\delta_1, m_\phi) \\
 &\quad + \sum_{\phi=\pi,K} \frac{g_3^2}{F_\phi^2} \xi_{B_6\phi,\delta_3}^{(3,c)} H_{B_6}^{(c)}(\delta_3, m_\phi) \\
 &\quad + \sum_{\phi=\pi,K,\eta} \frac{g_1^2}{F_\phi^2} \xi_{B_6\phi,\delta_1}^{(3,d)} H_{B_6}^{(d)}(0, m_\phi) \\
 &\quad + \sum_{\phi=\pi,K,\eta} \frac{g_2^2}{F_\phi^2} \xi_{B_6\phi,\delta_1}^{(3,d)} H_{B_6}^{(d)}(\delta_1, m_\phi) \\
 &\quad \left. + \sum_{\phi=\pi,K,\eta} \frac{g_3^2}{F_\phi^2} \xi_{B_6\phi,\delta_3}^{(3,e)} H_{B_6}^{(e)}(\delta_3, m_\phi) \right), \tag{6}
 \end{aligned}$$

with the coefficients $\xi_{B_{\bar{3}}\phi,\delta_i}^{(3;b,c,d,e)}$, $\xi_{B_6\phi,\delta_i}^{(3;b,c,d,e)}$ listed in Table III and Table IV. The explicit expressions of the loop functions $H_{B_{\bar{3}}}^{(b,c,d,e)}(\delta_i, m_\phi)$ and $H_{B_6}^{(b,c,d,e)}(\delta_i, m_\phi)$ can be found in the Appendix.

Once we obtain the loop functions in the EOMS scheme, we can easily obtain their HB counterparts by performing $1/m_0$ expansions. We have checked that our results agree with those of Ref. [23]. In the following section, for the sake of comparison, we study also the performance of the HBChPT in describing the lattice QCD data of Refs. [24–26]. It should be noted that in the following section, unless otherwise

stated, the HBChPT results refer to the ones obtained in the present work, not those of Ref. [23]

TABLE II: Coefficients of the tree level contributions of Eq. (5) for the B_6 states.

	Σ_c^{++}	Σ_c^+	Σ_c^0	$\Xi_c'^+$	$\Xi_c'^0$	Ω_c^0
α_6	1	$\frac{1}{2}$	0	$\frac{1}{2}$	0	0
β_6	1	1	1	1	1	1

TABLE III: Coefficients of the loop contributions of Eq. (6) for the $B_{\bar{3}}$ states.

	Λ_c^+	Ξ_c^+	Ξ_c^0
$\xi_{B_3\pi,\delta_1}^{(3,b)}$	0	1	-1
$\xi_{B_3K,\delta_1}^{(3,b)}$	1	0	-1
$\xi_{B_3\pi,\delta_2}^{(3,c)}$	0	1	-1
$\xi_{B_3K,\delta_2}^{(3,c)}$	1	0	-1
$\xi_{B_3\pi,\delta_1}^{(3,d)}$	6	$\frac{1}{2}$	1
$\xi_{B_3K,\delta_1}^{(3,d)}$	1	5	1
$\xi_{B_3\eta,\delta_1}^{(3,d)}$	0	$\frac{3}{2}$	0
$\xi_{B_3\pi,\delta_2}^{(3,e)}$	3	$\frac{1}{4}$	$\frac{1}{2}$
$\xi_{B_3K,\delta_2}^{(3,e)}$	$\frac{1}{2}$	$\frac{5}{2}$	$\frac{1}{2}$
$\xi_{B_3\eta,\delta_2}^{(3,e)}$	0	$\frac{3}{4}$	0

III. RESULTS AND DISCUSSIONS

In this section, we determine the LECs d_2 , d_3 , d_5 and d_6 by fitting to the lattice QCD data of Refs. [24–26], which are collected in Table V for the sake of easy reference. Because of the limited lattice QCD data, the other LECs g_{1-4} are fixed by the quark model and the heavy quark spin flavor symmetry. Their values are $g_1 = 0.98$, $g_2 = -\sqrt{\frac{3}{8}}g_1 = -0.60$, $g_3 = \frac{\sqrt{3}}{2}g_1 = 0.85$, and $g_4 = -\sqrt{3}g_2 = 1.04$ [50, 50, 51]. In our least-squares fit, the χ^2 as a function of the LECs is defined as

$$\chi^2(C_X) = \sum_{i=1}^n \frac{(\mu_i^{\text{th}}(C_X) - \mu_i^{\text{LQCD}})^2}{\sigma_i^2}, \quad (7)$$

where C_X denote all the LECs, σ_i correspond to the uncertainty of each lattice QCD datum, $\mu_i^{\text{th}}(C_X)$ and μ_i^{LQCD} stand for the magnetic moments obtained in the BChPT and those of the lattice QCD in Table V, respectively.

TABLE IV: Coefficients of the loop contributions of Eq. (6) for the B_6 states.

	Σ_c^{++}	Σ_c^+	Σ_c^0	$\Xi_c'^+$	$\Xi_c'^0$	Ω_c^0
$\xi_{B_6\pi}^{(3,b)}$	1	0	-1	$\frac{1}{2}$	$-\frac{1}{2}$	0
$\xi_{B_6K}^{(3,b)}$	1	$\frac{1}{2}$	0	0	$-\frac{1}{2}$	-1
$\xi_{B_6\pi,\delta_1}^{(3,b)}$	2	0	-2	1	-1	0
$\xi_{B_6K,\delta_1}^{(3,b)}$	2	1	0	0	-1	-2
$\xi_{B_6\pi,\delta_3}^{(3,c)}$	1	0	-1	$\frac{1}{2}$	$-\frac{1}{2}$	0
$\xi_{B_6K,\delta_3}^{(3,c)}$	1	$\frac{1}{2}$	0	0	$-\frac{1}{2}$	-1
$\xi_{B_6\pi}^{(3,d)}$	3	2	1	$\frac{1}{4}$	$\frac{1}{2}$	0
$\xi_{B_6K}^{(3,d)}$	1	$\frac{1}{2}$	0	$\frac{5}{2}$	$\frac{1}{2}$	1
$\xi_{B_6\eta}^{(3,d)}$	$\frac{2}{3}$	$\frac{1}{3}$	0	$\frac{1}{12}$	0	0
$\xi_{B_6\pi,\delta_1}^{(3,d)}$	2	2	2	$\frac{1}{2}$	1	0
$\xi_{B_6K,\delta_1}^{(3,d)}$	2	1	0	1	1	2
$\xi_{B_6\eta,\delta_1}^{(3,d)}$	0	0	0	$\frac{3}{2}$	0	0
$\xi_{B_6\pi,\delta_3}^{(3,e)}$	$\frac{3}{2}$	1	$\frac{1}{2}$	$\frac{1}{8}$	$\frac{1}{4}$	0
$\xi_{B_6K,\delta_3}^{(3,e)}$	$\frac{1}{2}$	$\frac{1}{4}$	0	$\frac{5}{4}$	$\frac{1}{4}$	$\frac{1}{2}$
$\xi_{B_6\eta,\delta_3}^{(3,e)}$	$\frac{1}{3}$	$\frac{1}{6}$	0	$\frac{1}{24}$	0	0

 TABLE V: Magnetic moments of singly charmed baryons at different m_π [24–27], in units of nuclear magneton [μ_N].

m_π (MeV)	Ξ_c^+	Ξ_c^0	Σ_c^{++}	Σ_c^0	$\Xi_c'^+$	$\Xi_c'^0$	Ω_c^0
Phys.	1.499(202)	-0.875(103)	-0.667(96)
156	0.235(25)	0.192(17)	0.315(141)	-0.599(71)	-0.688(31)
300	1.867(388)	-0.929(206)	-0.640(55)
410	1.591(358)	-0.897(223)	-0.621(44)
570	1.289(161)	-0.724(80)	-0.658(46)
700	1.447(125)	-0.757(67)	-0.701(56)

In order to decompose the contributions of loop diagrams, we will consider two cases. In case 1, all the allowed intermediate baryons are taken into account, while in case 2, only intermediate baryons of the same type as those of the external baryons are considered. Fitting to the lattice QCD data of Table V and with g_{1-4} fixed, the resulting LECs and χ^2 are listed in Table VI. One notes that the EOMS BChPT descriptions of the lattice QCD data are better than that of the HB BChPT in both cases.

TABLE VI: LECs d_2 , d_3 , d_5 , and d_6 determined by fitting to the lattice QCD data, with g_{1-4} fixed. In case 1 all the allowed intermediate baryons in the loop diagrams are taken into account, while in case 2 only intermediate baryons of the same type as those of the external baryons in the loop diagrams are considered.

	Case 1		Case 2	
	EOMS 1	HB 1	EOMS 2	HB 2
d_2	-1.25(15)	-2.32(15)	-1.78(15)	-1.78(15)
d_3	2.20(4)	0.65(4)	0.49(4)	0.49(4)
d_5	7.83(34)	13.49(34)	5.08(34)	8.69(34)
d_6	-3.76(5)	-4.93(5)	-2.66(5)	-3.40(5)
g_1	0.98	0.98	0.98	0.98
g_2	-0.60	0	-0.60	0
g_3	0.85	0.85	0.85	0.85
g_4	1.04	0	1.04	0
χ^2_{\min}	41.42	131.05	15.10	34.35

Note that we do not fit to the lattice QCD data obtained at $m_\pi = 700$ MeV, which are probably out of the range of validity of NLO ChPT. Furthermore, as can be seen in Fig. 3, the difference between the lattice QCD value and the ChPT prediction for $\mu_{\Xi_c'^0}$ is somehow relatively large. Thus, we do not include the lattice QCD magnetic moment of $\Xi_c'^0$ in our fitting as well.

For the sake of comparison with the lattice QCD data, in Fig. 2, we present the predicted magnetic moments of the singly charmed anti-triplet baryons as a function of m_π^2 . It is seen that the EOMS BChPT results are of the same quality as those of the HB BChPT for Ξ_c^+ and Ξ_c^0 . However, surprisingly, the EOMS and HB predictions for Λ_c^+ in case 1 are very different. From Table VII, we note that in the HBChPT the contributions from the intermediate anti-triplet and sextet baryons cancel each other at $O(p^3)$. Thus, at this order, loop corrections are quite small. But in the EOMS scheme, the loop contributions are rather large, especially for Λ_c^+ . In addition, we note that the main contributions of the loop diagrams are from the baryon pole diagram. Therefore, the large difference for the prediction of $\mu_{\Lambda_c^+}$ is caused by the absence of the baryon pole diagram in the HB BChPT at $O(p^3)$.

In Fig. 3, we plot the predicted magnetic moments of the singly charmed sextet baryons as a function of m_π^2 , in comparison with the lattice QCD data. The EOMS BChPT results are in better agreement with the lattice QCD data than those of the HB BChPT. As shown in Tables VI, on average the description of the lattice QCD data becomes worse if the intermediate anti-triplet states are included. Therefore, on average the results obtained in case 2 are in better agreement with the lattice QCD data. This has been noted in

Ref. [23] as well. In Tables VII and VIII, we decompose the loop contributions mediated by the $\bar{3}$, 6, and 6^* states. One can see that the convergence pattern in case 2 is in generally better than that in case 1, with probably the exception of Σ_c^0 . Therefore, we take the predictions obtained in case 2 as our final results.

In Fig. 4 and Fig. 5, we compare the predicted magnetic moments of all the singly charmed baryons at the physical point with those obtained in other approaches. We note that the results of different approaches are rather scattered. However, our results are in better agreement with those of the HBChPT of Ref. [23], though we have chosen different strategies to determine some of the LECs. Clearly, further experimental or lattice QCD studies are needed to pin down their values and to discriminate between different theoretical approaches.

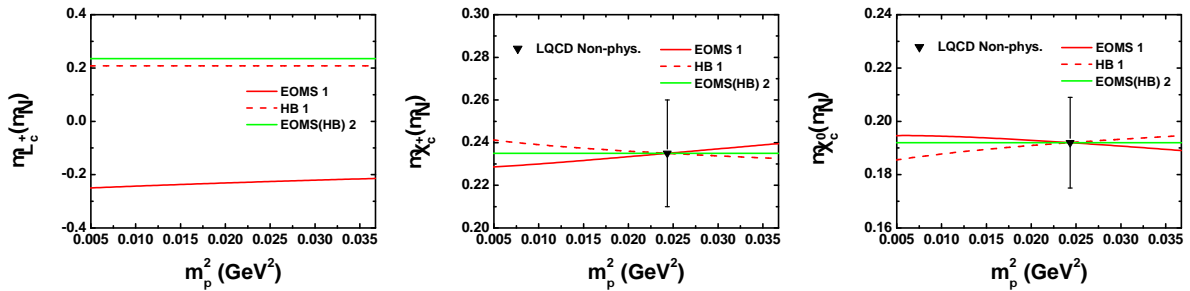


FIG. 2: Magnetic moments of the singly charmed anti-triplet baryons as a function of m_π^2 . The solid black nablas represent the corresponding lattice QCD data that are fitted.

TABLE VII: Decomposition of the loop contributions to the magnetic moments of singly charmed baryons. The subscript $\bar{3}$, 6, and 6^* denote the loop diagrams with the intermediate $\bar{3}$, 6, and 6^* states at $\mathcal{O}(p^3)$, respectively.

EOMS 1					HB 1					LQCD [24, 27]		
	$\mathcal{O}(p^2)$	$\mathcal{O}(p^3)_{\bar{3}}$	$\mathcal{O}(p^3)_6$	$\mathcal{O}(p^3)_{6^*}$	μ_{tot}		$\mathcal{O}(p^2)$	$\mathcal{O}(p^3)_{\bar{3}}$	$\mathcal{O}(p^3)_6$	$\mathcal{O}(p^3)_{6^*}$	μ_{tot}	
$B_{\bar{3}}$	$\mu_{\Lambda_c^+}$	1.005	...	0.035	-1.272	-0.232	0.191	...	-0.263	0.280	0.208	...
	$\mu_{\Xi_c^+}$	1.005	...	0.141	-0.913	0.233	0.191	...	-0.169	0.215	0.237	...
	$\mu_{\Xi_c^0}$	0.859	...	0.330	-0.996	0.193	0.253	...	0.432	-0.495	0.190	...
	$\mu_{\Sigma_c^{++}}$	2.251	-0.293	-0.444	0.090	1.604	3.916	-0.319	-0.988	0.288	2.897	1.499(202)
	$\mu_{\Sigma_c^+}$	0.428	-0.192	-0.094	-0.042	0.100	1.044	-0.243	-0.349	0.091	0.543	...
	$\mu_{\Sigma_c^0}$	-1.394	-0.090	0.256	-0.175	-1.403	-1.828	-0.168	0.290	-0.106	-1.812	-0.875(103)
B_6	$\mu_{\Xi_c^{'+}}$	0.428	0.067	0.112	-0.048	0.559	1.044	0.084	-0.145	0.053	1.036	...
	$\mu_{\Xi_c'^0}$	-1.394	0.135	0.380	-0.198	-1.077	-1.828	0.159	0.494	-0.144	-1.319	...
	$\mu_{\Omega_c^0}$	-1.394	0.361	0.505	-0.220	-0.748	-1.828	0.486	0.698	-0.182	-0.826	-0.667(96)

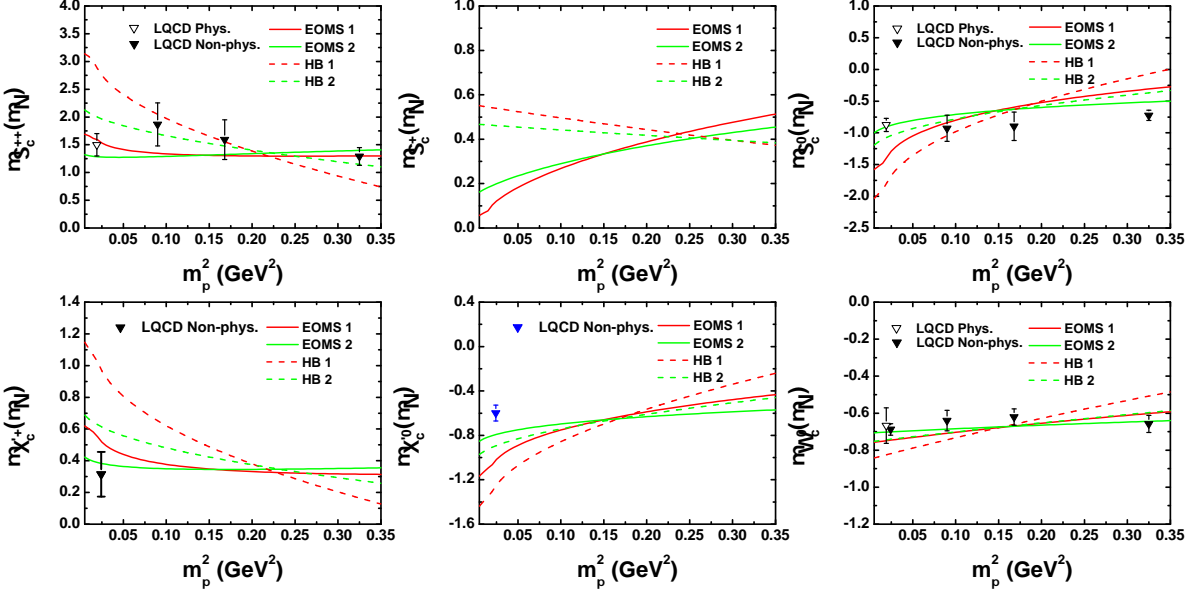


FIG. 3: Magnetic moments of the singly charmed sextet baryons as a function of m_π^2 . The solid black nablas refer to the corresponding lattice QCD data fitted. The hollow nablas stand for the lattice QCD physical values. The blue nablas denote the lattice QCD data not used in our fitting.

TABLE VIII: Same as Table VII , but for case 2.

	EOMS 2					HB 2					LQCD [24, 27]	
	$O(p^2)$	$O(p^3)_{\bar{3}}$	$O(p^3)_6$	$O(p^3)_{6^*}$	μ_{tot}	$O(p^2)$	$O(p^3)_{\bar{3}}$	$O(p^3)_6$	$O(p^3)_{6^*}$	μ_{tot}		
$\mu_{\Lambda_c^+}$	0.235	0.235	0.235	0.235
B_3	$\mu_{\Xi_c^+}$	0.235	0.235	0.235	0.235
	$\mu_{\Xi_c^0}$	0.192	0.192	0.192	0.192
	$\mu_{\Sigma_c^{++}}$	1.639	...	-0.444	0.090	1.285	2.703	...	-0.988	0.288	2.003	1.499(202)
B_6	$\mu_{\Sigma_c^+}$	0.326	...	-0.094	-0.042	0.190	0.721	...	-0.349	0.091	0.463	...
	$\mu_{\Sigma_c^0}$	-0.986	...	0.256	-0.175	-0.905	-1.261	...	0.290	-0.106	-1.077	-0.875(103)
	$\mu_{\Xi_c^{'+}}$	0.326	...	0.112	-0.048	0.390	0.721	...	-0.145	0.053	0.629	...
	$\mu_{\Xi_c^{'0}}$	-0.986	...	0.380	-0.197	-0.803	-1.261	...	0.494	-0.144	-0.911	...
	$\mu_{\Omega_c^0}$	-0.986	...	0.504	-0.220	-0.702	-1.261	...	0.698	-0.182	-0.745	-0.667(96)

IV. SUMMARY

Motivated by the recent experimental progress on heavy flavor hadrons, we have studied the magnetic moments of the singly charmed baryons in the covariant baryon chiral perturbation theory (BChPT) up to

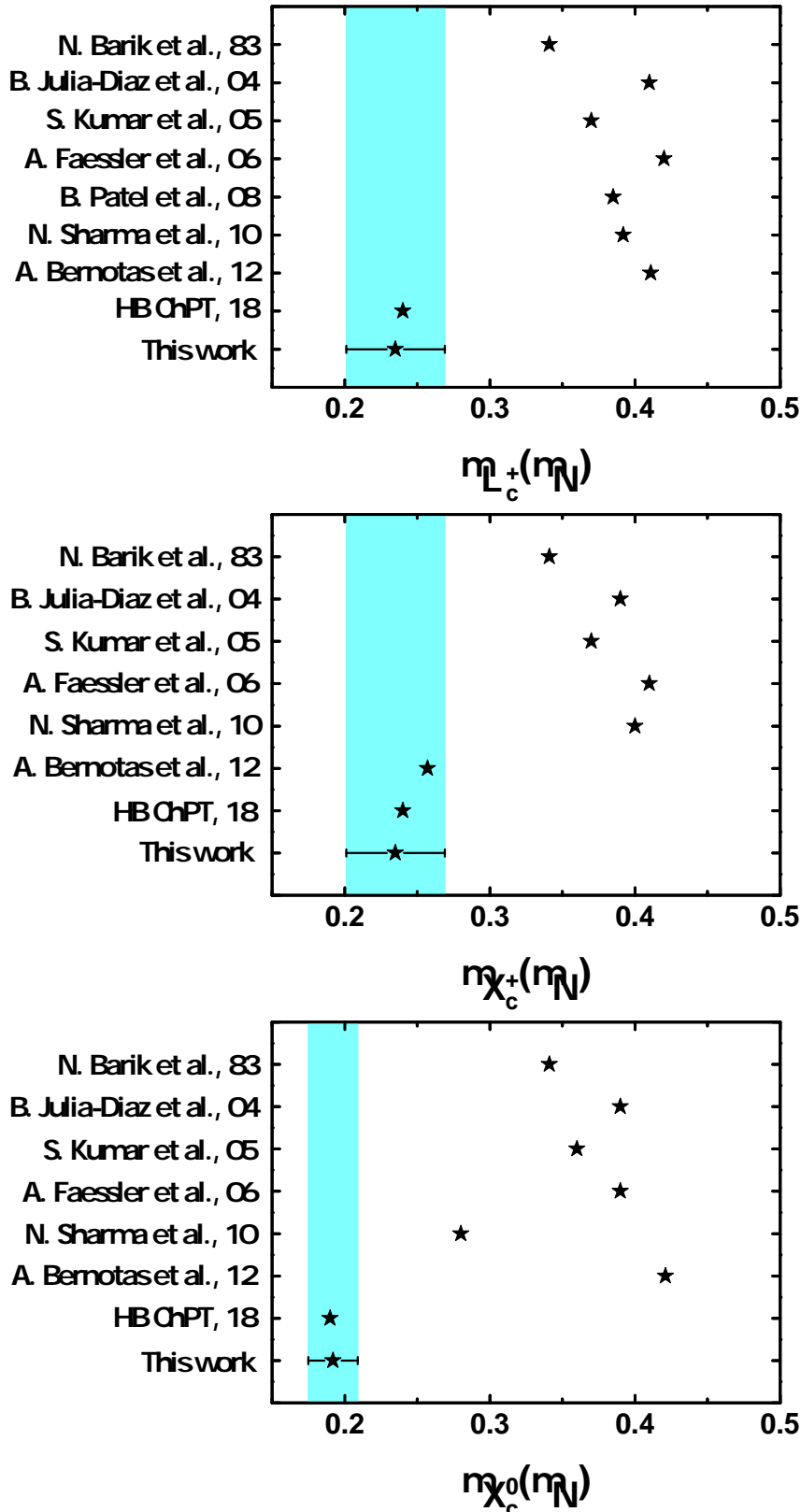


FIG. 4: Magnetic moments of the anti-triplet baryons obtained in different approaches. The light-blue bands represent the result obtained in the present work. The others are taken from Ref. [13] (N. Barik et al., 83), Ref. [14] (B. Julia-Diaz et al., 04), Ref. [15] (S. Kumar et al., 05), Ref. [16] (A. Faessler et al., 06), Ref. [17] (B. Patel et al., 08), Ref. [18] (N. Sharma et al., 10), Ref. [19] (A. Bernotas et al., 12), and Ref. [23] (HB ChPT, 18).

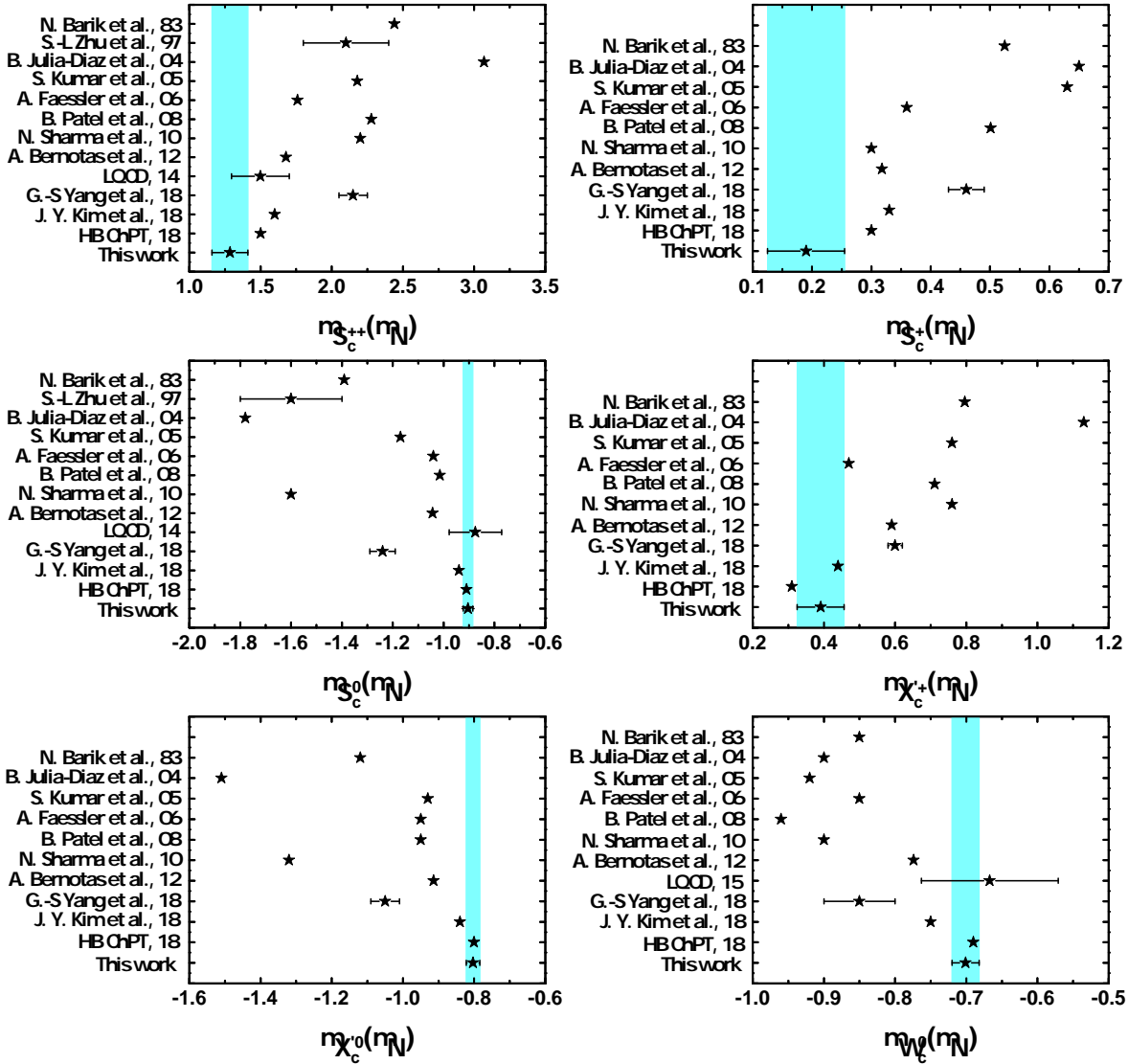


FIG. 5: Same as Fig. 4, but for the sextet baryons. Additional data are taken from Ref. [20] (S.-L Zhu et al., 97), Ref. [21] (G.-S Yang et al., 18), Ref. [22] (J. Y. Kim et al., 18), Ref. [24] (LQCD, 14), and Ref. [27] (LQCD, 15).

the next-to-leading order. Using the quark model and the heavy quark spin flavor symmetry to fix some of

the low energy constants, we determined the rest by fitting to the lattice QCD data. We compared our results with those of the heavy baryon (HB) ChPT and found that on average the lattice QCD quark mass dependent data can be better described by the covariant BChPT, consistent with previous studies. In addition, we found that the baryon pole diagram, which is absent in the HB ChPT, can play an important role in certain cases.

Compared with the results of other approaches, our predicted magnetic moments for the anti-triplets are relatively small. The same is true for the Σ_c^{++} , Σ_c^+ , and $\Xi_c^{\prime+}$. On the other hand, our results for Σ_c^0 , $\Xi_c^{\prime 0}$, and Ω_c^0 are relatively large (small in absolute value). It is not clear how to understand such a pattern at present. We hope that future lattice QCD or experimental studies can help us gain more insight into these important quantities and better understand the singly charmed baryons.

V. ACKNOWLEDGEMENTS

RXS thanks Jun-Xu Lu and Xiu-Lei Ren for useful discussions. This work is partly supported by the National Natural Science Foundation of China under Grants No.11522539, No. 11735003, and the fundamental Research Funds for the Central Universities.

VI. APPENDIX

The pertinent loop functions, with the PCB terms removed, are given here.

[1] M. Tanabashi *et al.* [Particle Data Group], Phys. Rev. D **98**, 030001 (2018).

$$\begin{aligned}
H_{B_3}^{(b)}(\delta_1, m_\phi) &= H^{(b)}(m_{\bar{3}}, \delta_1, m_\phi), & H_{B_3}^{(d)}(\delta_1, m_\phi) &= H^{(d)}(m_{\bar{3}}, \delta_1, m_\phi), \\
H_{B_3}^{(c)}(\delta_2, m_\phi) &= \begin{cases} H_{\delta < m_\phi}^{(c)}(m_{\bar{3}}, \delta_2, m_\phi), & (\delta_2 < m_\phi) \\ H_{\delta > m_\phi}^{(c)}(m_{\bar{3}}, \delta_2, m_\phi), & (\delta_2 > m_\phi) \end{cases} \\
H_{B_3}^{(e)}(\delta_2, m_\phi) &= \begin{cases} H_{\delta < m_\phi}^{(e)}(m_{\bar{3}}, \delta_2, m_\phi), & (\delta_2 < m_\phi) \\ H_{\delta > m_\phi}^{(e)}(m_{\bar{3}}, \delta_2, m_\phi), & (\delta_2 > m_\phi) \end{cases} \\
H_{B_6}^{(b)}(0, m_\phi) &= H^{(b)}(m_6, 0, m_\phi), & H_{B_6}^{(b)}(\delta_1, m_\phi) &= H^{(b)}(m_6, -\delta_1, m_\phi) \\
H_{B_6}^{(d)}(0, m_\phi) &= H^{(d)}(m_6, 0, m_\phi), & H_{B_6}^{(d)}(\delta_1, m_\phi) &= H^{(d)}(m_6, -\delta_1, m_\phi) \\
H_{B_6}^{(c)}(\delta_3, m_\phi) &= H_{\delta < m_\phi}^{(c)}(m_6, \delta_3, m_\phi), & (\delta_3 < m_\phi) \\
H_{B_6}^{(e)}(\delta_3, m_\phi) &= H_{\delta < m_\phi}^{(e)}(m_6, \delta_3, m_\phi), & (\delta_3 < m_\phi)
\end{aligned} \tag{8}$$

$$H^{(b)}(m_B, 0, m_\phi) = -\frac{1}{4\pi^2} \left[2m_\phi^2 + \frac{m_\phi^2}{m_B^2} (2m_B^2 - m_\phi^2) \log\left(\frac{m_\phi^2}{m_B^2}\right) + \frac{2m_\phi(m_\phi^4 - 4m_\phi^2 m_B^2 + 2m_B^2)}{m_B^2 \sqrt{4m_B^2 - m_\phi^2}} \arccos\left(\frac{m_\phi}{2m_B}\right) \right], \tag{9}$$

$$\begin{aligned}
H^{(b)}(m_B, \delta, m_\phi) &= \frac{m_B}{8\pi^2} \int_0^1 dx \int_0^{1-x} dy \left\{ \frac{x^4 m_B^3 + \delta x^3 m_B^2}{x(m_B + \delta)^2 + (x-1)(xm_B^2 - m_\phi^2)} \right. \\
&\quad + \left[(4x^2 + 4x - 2)m_B + \delta(3x - 1) \right] \log\left(\frac{x(m_B + \delta)^2 + (x-1)(xm_B^2 - m_\phi^2)}{\mu^2}\right) \\
&\quad \left. - 2(2x^2 + 2x - 1)m_B \log\left(\frac{x^2 m_B^2}{\mu^2}\right) - x^2 m_B - \delta + 4\delta x \right\}, \quad (0 < \delta < m_\phi)
\end{aligned} \tag{10}$$

$$H^{(d)}(m_B, 0, m_\phi) = -\frac{1}{4\pi^2} \left[2m_\phi^2 + \frac{m_\phi^2}{m_B^2} (m_B^2 - m_\phi^2) \log\left(\frac{m_\phi^2}{m_B^2}\right) + \frac{2m_\phi^3(m_\phi^2 - 3m_B^2)}{m_B^2 \sqrt{4m_B^2 - m_\phi^2}} \arccos\left(\frac{m_\phi}{2m_B}\right) \right], \tag{11}$$

$$\begin{aligned}
H^{(d)}(m_B, \delta, m_\phi) &= -\frac{(2m_B + \delta)^2}{16\pi^2 m_B^4} \left\{ 2 \left[m_B^2 (m_\phi^2 - 2\delta^2) + 3\delta m_B (m_\phi - \delta) (\delta + m_\phi) - (m_\phi^2 - \delta^2)^2 \right] \log\left(\frac{m_\phi}{m_B + \delta}\right) \right. \\
&\quad - 2 \sqrt{\frac{(m_\phi - \delta)(\delta + m_\phi)}{(2m_B + \delta - m_\phi)(2m_B + \delta + m_\phi)}} \left[m_B^2 (8\delta^2 - 3m_\phi^2) + 5\delta m_B (\delta^2 - m_\phi^2) + 4\delta m_B^3 \right. \\
&\quad \left. + (m_\phi^2 - \delta^2)^2 \right] \tan^{-1} \left(\frac{-2\delta m_B - 2m_B^2 - \delta^2 + m_\phi^2}{\sqrt{(m_\phi - \delta)(\delta + m_\phi)(2m_B + \delta - m_\phi)(2m_B + \delta + m_\phi)}} \right) \\
&\quad + 2 \left[m_B^2 (8\delta^2 - 3m_\phi^2) + 5\delta m_B (\delta^2 - m_\phi^2) + 4\delta m_B^3 + (m_\phi^2 - \delta^2)^2 \right] \\
&\quad \cdot \sqrt{\frac{(m_\phi - \delta)(\delta + m_\phi)}{(2m_B + \delta - m_\phi)(2m_B + \delta + m_\phi)}} \\
&\quad \cdot \tan^{-1} \left(\frac{m_\phi^2 - \delta(2m_B + \delta)}{\sqrt{(m_\phi - \delta)(\delta + m_\phi)(2m_B + \delta - m_\phi)(2m_B + \delta + m_\phi)}} \right) \\
&\quad \left. + m_B^2 \left[-2\delta m_B + m_B^2 + 2(m_\phi - \delta)(\delta + m_\phi) \right] \right\} + \frac{m_B^2}{4\pi^2},
\end{aligned} \tag{12}$$

$$\begin{aligned}
& H_{\delta < m_\phi}^{(c)}(m_B, \delta, m_\phi) \\
= & \frac{1}{864\pi^2 m_B^4 (\delta + m_B)^2} \left\{ -30 \log\left(\frac{\delta + m_B}{m_\phi}\right) m_\phi^8 - 6 \left[\left(38 \log\left(\frac{m_\phi}{\delta + m_B}\right) + 5 \right) m_B^2 \right. \right. \\
& + 5 \left(\tan^{-1} \left(\frac{\delta^2 + 2m_B\delta - m_\phi^2}{\sqrt{((\delta + 2m_B)^2 - m_\phi^2)(m_\phi^2 - \delta^2)}} \right) - \tan^{-1} \left(\frac{\delta^2 + 2m_B\delta + 2m_B^2 - m_\phi^2}{\sqrt{((\delta + 2m_B)^2 - m_\phi^2)(m_\phi^2 - \delta^2)}} \right) \right) \\
& \cdot \sqrt{((\delta + 2m_B)^2 - m_\phi^2)(m_\phi^2 - \delta^2)} - 4\delta \log\left(\frac{\delta + m_B}{m_\phi}\right) (5\delta + 11m_B) \left. m_\phi^6 \right] \\
& + 3 \left[-4 \log\left(\frac{\delta + m_B}{m_\phi}\right) (15\delta^2 + 66m_B\delta + 79m_B^2) \delta^2 + 2 \left(\tan^{-1} \left(\frac{\delta^2 + 2m_B\delta - m_\phi^2}{\sqrt{((\delta + 2m_B)^2 - m_\phi^2)(m_\phi^2 - \delta^2)}} \right) \right. \right. \\
& - \tan^{-1} \left(\frac{\delta^2 + 2m_B\delta + 2m_B^2 - m_\phi^2}{\sqrt{((\delta + 2m_B)^2 - m_\phi^2)(m_\phi^2 - \delta^2)}} \right) \left. \right) \sqrt{((\delta + 2m_B)^2 - m_\phi^2)(m_\phi^2 - \delta^2)} \\
& \cdot (15\delta^2 + 34m_B\delta + 28m_B^2) + m_B^2 \left(30\delta^2 + 68m_B\delta + 61m_B^2 + 2 \log\left(\frac{m_\phi}{\delta + m_B}\right) \right. \\
& \cdot (76\delta^2 + 195m_B\delta + 75m_B^2) \left. \right] m_\phi^4 \\
& + 2 \left[30 \log(\delta + m_B) (12\delta + m_B) m_B^5 - (45\delta^4 + 204m_B\delta^3 + 354m_B^2\delta^2 + 267m_B^3\delta + 92m_B^4) m_B^2 \right. \\
& + 3 \left(\tan^{-1} \left(\frac{\delta^2 + 2m_B\delta + 2m_B^2 - m_\phi^2}{\sqrt{((\delta + 2m_B)^2 - m_\phi^2)(m_\phi^2 - \delta^2)}} \right) - \tan^{-1} \left(\frac{\delta^2 + 2m_B\delta - m_\phi^2}{\sqrt{((\delta + 2m_B)^2 - m_\phi^2)(m_\phi^2 - \delta^2)}} \right) \right) \\
& \sqrt{((\delta + 2m_B)^2 - m_\phi^2)(m_\phi^2 - \delta^2)} (15\delta^4 + 68m_B\delta^3 + 118m_B^2\delta^2 + 91m_B^3\delta + 29m_B^4) \\
& + 3 \left(-2 \log\left(\frac{1}{\mu^2}\right) (3\delta + 2m_B) m_B^5 - 6 \log(m_\phi) (22\delta + 3m_B) m_B^5 \right. \\
& - \delta^3 \log\left(\frac{m_\phi}{\delta + m_B}\right) (38\delta + 195m_B) m_B^2 + \delta^2 \log\left(\frac{\delta + m_B}{m_\phi}\right) \\
& \cdot (20\delta^4 + 132m_B\delta^3 + 316m_B^2\delta^2 + 295m_B^3\delta + 360m_B^4) \left. \right] m_\phi^2 \\
& \left[-72\delta \log(m_\phi) m_B^6 (\delta + 2m_B) + 60 \log(\delta + m_B) m_B^6 (2\delta + m_B) (\delta + 2m_B) \right. \\
& + 6 \log\left(\frac{1}{\mu^2}\right) m_B^6 (\delta + 2m_B) (4\delta + 5m_B) + 30\delta^3 \log\left(\frac{m_\phi}{\delta + m_B}\right) m_B^4 (59\delta + 26m_B) \\
& - 6\delta^5 \log\left(\frac{\delta + m_B}{m_\phi}\right) (5\delta^3 + 44m_B\delta^2 + 158m_B^2\delta + 295m_B^3) \\
& + 6 \left(\tan^{-1} \left(\frac{\delta^2 + 2m_B\delta - m_\phi^2}{\sqrt{((\delta + 2m_B)^2 - m_\phi^2)(m_\phi^2 - \delta^2)}} \right) - \tan^{-1} \left(\frac{\delta^2 + 2m_B\delta + 2m_B^2 - m_\phi^2}{\sqrt{((\delta + 2m_B)^2 - m_\phi^2)(m_\phi^2 - \delta^2)}} \right) \right) \\
& \cdot \sqrt{((\delta + 2m_B)^2 - m_\phi^2)(m_\phi^2 - \delta^2)} (\delta + 2m_B)^2 (5\delta^4 + 14m_B\delta^3 + 14m_B^2\delta^2 + 3m_B^3\delta - 3m_B^4) \\
& + m_B^2 (30\delta^6 + 204m_B\delta^5 + 525m_B^2\delta^4 + 618m_B^3\delta^3 + 250m_B^4\delta^2 - 110m_B^5\delta - 86m_B^6) \left. \right] \\
& - \frac{m_B^2 \left(30 \log\left(\frac{m_B^2}{\mu^2}\right) - 43 \right)}{432\pi^2}, \tag{13}
\end{aligned}$$

$$\begin{aligned}
& H_{\delta > m_\phi}^{(c)}(m_B, \delta, m_\phi) \\
= & \frac{1}{864\pi^2 m_B^4 (\delta + m_B)^2} \left\{ -30 \log\left(\frac{\delta + m_B}{m_\phi}\right) m_\phi^8 - 6 \left[\left(38 \log\left(\frac{m_\phi}{\delta + m_B}\right) + 5 \right) m_B^2 \right. \right. \\
& + 5 \coth^{-1} \left(\frac{m_\phi^2 + \delta(\delta + 2m_B)}{\sqrt{(\delta^2 - m_\phi^2)((\delta + 2m_B)^2 - m_\phi^2)}} \right) \sqrt{(\delta^2 - m_\phi^2)((\delta + 2m_B)^2 - m_\phi^2)} \\
& \left. \left. - 4\delta \log\left(\frac{\delta + m_B}{m_\phi}\right) (5\delta + 11m_B) \right] m_\phi^6 \right. \\
& + 3 \left[-4 \log\left(\frac{\delta + m_B}{m_\phi}\right) (15\delta^2 + 66m_B\delta + 79m_B^2) \delta^2 + 2 \coth^{-1} \left(\frac{m_\phi^2 + \delta(\delta + 2m_B)}{\sqrt{(\delta^2 - m_\phi^2)((\delta + 2m_B)^2 - m_\phi^2)}} \right) \right. \\
& \cdot \sqrt{(\delta^2 - m_\phi^2)((\delta + 2m_B)^2 - m_\phi^2)} (15\delta^2 + 34m_B\delta + 28m_B^2) + m_B^2 (30\delta^2 + 68m_B\delta + 61m_B^2 \\
& \left. \left. + 2 \log\left(\frac{m_\phi}{\delta + m_B}\right) (76\delta^2 + 195m_B\delta + 75m_B^2) \right] m_\phi^4 \right. \\
& + 2 \left[30 \log(\delta + m_B) m_B^6 - (45\delta^4 + 204m_B\delta^3 + 354m_B^2\delta^2 + 267m_B^3\delta + 92m_B^4) m_B^2 \right. \\
& - 3 \coth^{-1} \left(\frac{m_\phi^2 + \delta(\delta + 2m_B)}{\sqrt{(\delta^2 - m_\phi^2)((\delta + 2m_B)^2 - m_\phi^2)}} \right) (15\delta^4 + 68m_B\delta^3 + 118m_B^2\delta^2 + 91m_B^3\delta + 29m_B^4) \\
& \cdot \sqrt{(\delta^2 - m_\phi^2)((\delta + 2m_B)^2 - m_\phi^2)} + 3 \left(20 \log\left(\frac{\delta + m_B}{m_\phi}\right) \delta^6 + 132 \log\left(\frac{\delta + m_B}{m_\phi}\right) m_B \delta^5 \right. \\
& + 316 \log\left(\frac{\delta + m_B}{m_\phi}\right) m_B^2 \delta^4 + 295 \log\left(\frac{\delta + m_B}{m_\phi}\right) m_B^3 \delta^3 - \log\left(\frac{m_\phi}{\delta + m_B}\right) m_B^2 (38\delta + 195m_B) \delta^3 \\
& \left. \left. + 360 \log\left(\frac{\delta + m_B}{m_\phi}\right) m_B^4 \delta^2 - 6 \log\left(\frac{(\delta + m_B)^2}{\mu^2}\right) m_B^5 \delta + 132 \log\left(\frac{\delta + m_B}{m_\phi}\right) m_B^5 \delta \right. \\
& \left. - 4 \log\left(\frac{1}{\mu^2}\right) m_B^6 - 18 \log(m_\phi) m_B^6 \right] m_\phi^2 \right. \\
& + 60\delta \log(\delta + m_B) m_B^6 (2\delta + 5m_B) + 6 \coth^{-1} \left(\frac{m_\phi^2 + \delta(\delta + 2m_B)}{\sqrt{(\delta^2 - m_\phi^2)((\delta + 2m_B)^2 - m_\phi^2)}} \right) \\
& \sqrt{(\delta^2 - m_\phi^2)((\delta + 2m_B)^2 - m_\phi^2)} (\delta + 2m_B)^2 (5\delta^4 + 14m_B\delta^3 + 14m_B^2\delta^2 + 3m_B^3\delta - 3m_B^4) \\
& + m_B^2 (30\delta^6 + 204m_B\delta^5 + 525m_B^2\delta^4 + 618m_B^3\delta^3 + 250m_B^4\delta^2 - 110m_B^5\delta - 86m_B^6) \\
& + 6 \left[10 \log\left(\frac{(\delta + m_B)^2}{\mu^2}\right) m_B^8 - 12\delta \log(m_\phi) (\delta + 2m_B) m_B^6 + \delta \log\left(\frac{1}{\mu^2}\right) (4\delta + 13m_B) m_B^6 \right. \\
& \left. + 5\delta^3 \log\left(\frac{m_\phi}{\delta + m_B}\right) (59\delta + 26m_B) m_B^4 - \delta^5 \log\left(\frac{\delta + m_B}{m_\phi}\right) (5\delta^3 + 44m_B\delta^2 + 158m_B^2\delta + 295m_B^3) \right] \right\} \\
& - \frac{m_B^2 \left(30 \log\left(\frac{m_\phi^2}{\mu^2}\right) - 43 \right)}{432\pi^2}, \tag{14}
\end{aligned}$$

$$\begin{aligned}
H_{\delta < m_\phi}^{(e)}(m_B, \delta, m_\phi) = & \frac{\left(80 \log\left(\frac{m_B^2}{\mu^2}\right) - 3\right) m_B^2}{432\pi^2} + \frac{1}{432\pi^2 (\delta + m_B)^4 m_B^4} \left\{ \left[-2 \log\left(\frac{\delta + m_B}{m_\phi}\right) (9\delta^2 + 22m_B\delta + 16m_B^2) \right] m_\phi^8 \right. \\
& + 2 \left[- \left(9 \left(28 \log\left(\frac{m_\phi}{\delta + m_B}\right) + 1 \right) \delta^2 + 22m_B\delta + 16m_B^2 \right) m_B^2 \right. \\
& + \left(\tan^{-1}\left(\frac{\delta^2 + 2m_B\delta + 2m_B^2 - m_\phi^2}{\sqrt{((\delta + 2m_B)^2 - m_\phi^2)(m_\phi^2 - \delta^2)}}\right) - \tan^{-1}\left(\frac{\delta^2 + 2m_B\delta - m_\phi^2}{\sqrt{((\delta + 2m_B)^2 - m_\phi^2)(m_\phi^2 - \delta^2)}}\right) \right) \\
& \cdot \sqrt{((\delta + 2m_B)^2 - m_\phi^2)(m_\phi^2 - \delta^2)} (9\delta^2 + 22m_B\delta + 16m_B^2) \\
& + 4 \log\left(\frac{\delta + m_B}{m_\phi}\right) (9\delta^4 + 40m_B\delta^3 + 8m_B^2\delta^2 + 62m_B^3\delta + 25m_B^4) \Big] m_\phi^6 \\
& + \left[16\delta^2 \log\left(\frac{m_\phi}{\delta + m_B}\right) (63\delta^2 + 137m_B\delta + 135m_B^2) m_B^2 \right. \\
& + (54\delta^4 + 240m_B\delta^3 + 421m_B^2\delta^2 + 330m_B^3\delta + 84m_B^4) m_B^2 \\
& + 2 \left(\tan^{-1}\left(\frac{\delta^2 + 2m_B\delta - m_\phi^2}{\sqrt{((\delta + 2m_B)^2 - m_\phi^2)(m_\phi^2 - \delta^2)}}\right) - \tan^{-1}\left(\frac{\delta^2 + 2m_B\delta + 2m_B^2 - m_\phi^2}{\sqrt{((\delta + 2m_B)^2 - m_\phi^2)(m_\phi^2 - \delta^2)}}\right) \right) \\
& \cdot \sqrt{((\delta + 2m_B)^2 - m_\phi^2)(m_\phi^2 - \delta^2)} (27\delta^4 + 120m_B\delta^3 + 206m_B^2\delta^2 + 172m_B^3\delta + 68m_B^4) \\
& - 4 \left(-204\delta \log(m_\phi) m_B^5 + 60 \log(\delta + m_B) (4\delta + m_B) m_B^5 + 6 \log\left(\frac{1}{\mu^2}\right) (3\delta + 5m_B) m_B^5 \right. \\
& \left. + \delta^3 \log\left(\frac{\delta + m_B}{m_\phi}\right) (27\delta^3 + 174m_B\delta^2 + 216m_B^2\delta + 124m_B^3) \right] m_\phi^4 \\
& - 2 \left[20 \log(\delta + m_B) (-85\delta^3 - 27m_B\delta^2 + 2m_B^2\delta + 2m_B^3) m_B^5 \right. \\
& + (27\delta^6 + 174m_B\delta^5 + 454m_B^2\delta^4 + 612m_B^3\delta^3 + 422m_B^4\delta^2 + 110m_B^5\delta - 6m_B^6) m_B^2 \\
& + \left(\tan^{-1}\left(\frac{\delta^2 + 2m_B\delta - m_\phi^2}{\sqrt{((\delta + 2m_B)^2 - m_\phi^2)(m_\phi^2 - \delta^2)}}\right) - \tan^{-1}\left(\frac{\delta^2 + 2m_B\delta + 2m_B^2 - m_\phi^2}{\sqrt{((\delta + 2m_B)^2 - m_\phi^2)(m_\phi^2 - \delta^2)}}\right) \right) \\
& \cdot \sqrt{((\delta + 2m_B)^2 - m_\phi^2)(m_\phi^2 - \delta^2)} (\delta + 2m_B) (27\delta^5 + 120m_B\delta^4 + 214m_B^2\delta^3 + 172m_B^3\delta^2 + 50m_B^4\delta + 8m_B^5) \\
& + 4 \left(\log\left(\frac{m_\phi}{\delta + m_B}\right) m_B^2 (63\delta + 274m_B) \delta^5 - \log\left(\frac{\delta + m_B}{m_\phi}\right) (9\delta^4 + 76m_B\delta^3 + 208m_B^2\delta^2 + 257m_B^3\delta + 620m_B^4) \delta^4 \right. \\
& \left. + \log\left(\frac{1}{\mu^2}\right) m_B^5 (9\delta^3 + 36m_B\delta^2 + 41m_B^2\delta + 11m_B^3) + \log(m_\phi) m_B^5 (443\delta^3 + 207m_B\delta^2 + 72m_B^2\delta + 12m_B^3) \right] m_\phi^2 \\
& + \left[3180\delta^6 \log\left(\frac{m_\phi}{\delta + m_B}\right) m_B^4 + 32\delta^2 \log(m_\phi) m_B^5 (103\delta^3 + 73m_B\delta^2 + 32m_B^2\delta + 6m_B^3) \right. \\
& - 2\delta^7 \log\left(\frac{\delta + m_B}{m_\phi}\right) (9\delta^3 + 94m_B\delta^2 + 416m_B^2\delta + 1028m_B^3) \\
& + 2\delta \left(\tan^{-1}\left(\frac{\delta^2 + 2m_B\delta - m_\phi^2}{\sqrt{((\delta + 2m_B)^2 - m_\phi^2)(m_\phi^2 - \delta^2)}}\right) - \tan^{-1}\left(\frac{\delta^2 + 2m_B\delta + 2m_B^2 - m_\phi^2}{\sqrt{((\delta + 2m_B)^2 - m_\phi^2)(m_\phi^2 - \delta^2)}}\right) \right) \\
& \cdot \sqrt{((\delta + 2m_B)^2 - m_\phi^2)(m_\phi^2 - \delta^2)} (\delta + 2m_B)^3 (9\delta^4 + 22m_B\delta^3 + 24m_B^2\delta^2 + 20m_B^3\delta + 6m_B^4) \\
& - 2 \log\left(\frac{1}{\mu^2}\right) m_B^5 (\delta + 2m_B) (36\delta^4 + 144m_B\delta^3 + 196m_B^2\delta^2 + 105m_B^3\delta + 20m_B^4) \\
& - 20 \log(\delta + m_B) m_B^5 (172\delta^5 + 160m_B\delta^4 + 148m_B^2\delta^3 + 109m_B^3\delta^2 + 46m_B^4\delta + 8m_B^5) \\
& + m_B^2 (18\delta^8 + 152m_B\delta^7 + 519m_B^2\delta^6 + 918m_B^3\delta^5 + 954m_B^4\delta^4 + 688m_B^5\delta^3 + 382m_B^6\delta^2 + 116m_B^7\delta + 3m_B^8) \Big], \\
\end{aligned} \tag{15}$$

$$\begin{aligned}
H_{\delta>m_\phi}^{(e)}(m_B, \delta, m_\phi) = & \frac{\left(80 \log \left(\frac{m_B^2}{\mu^2}\right)-3\right) m_B^2}{432 \pi^2} + \frac{1}{432 \pi^2 (\delta+m_B)^4 m_B^4} \left\{ \left[-2 \log \left(\frac{\delta+m_B}{m_\phi}\right) (9 \delta^2 + 22 m_B \delta + 16 m_B^2) \right] m_\phi^8 \right. \\
& + 2 \left[-4 \log \left(\frac{m_\phi}{\delta+m_B}\right) (9 \delta + 40 m_B) \delta^3 - \coth^{-1} \left(\frac{\delta^2 + 2 m_B \delta + m_\phi^2}{\sqrt{(\delta^2 - m_\phi^2)((\delta+2m_B)^2 - m_\phi^2)}} \right) (9 \delta^2 + 22 m_B \delta + 16 m_B^2) \right. \\
& \cdot \sqrt{(\delta^2 - m_\phi^2)((\delta+2m_B)^2 - m_\phi^2)} \\
& + m_B^2 \left(-9 \delta^2 - 22 m_B \delta - 16 m_B^2 + 4 \log \left(\frac{\delta+m_B}{m_\phi}\right) (71 \delta^2 + 62 m_B \delta + 25 m_B^2) \right] m_\phi^6 \\
& + \left[\left(54 \delta^4 + 240 m_B \delta^3 + 421 m_B^2 \delta^2 + 16 \log \left(\frac{m_\phi}{\delta+m_B}\right) (117 \delta^2 + 137 m_B \delta + 135 m_B^2) \delta^2 \right. \right. \\
& + 330 m_B^3 \delta + 84 m_B^4 - 24 \log \left(\frac{m_\phi^2}{\mu^2}\right) m_B^3 (3 \delta + 5 m_B) \left. \right] m_B^2 \\
& + 2 \coth^{-1} \left(\frac{\delta^2 + 2 m_B \delta + m_\phi^2}{\sqrt{(\delta^2 - m_\phi^2)((\delta+2m_B)^2 - m_\phi^2)}} \right) \sqrt{(\delta^2 - m_\phi^2)((\delta+2m_B)^2 - m_\phi^2)} \\
& \cdot (27 \delta^4 + 120 m_B \delta^3 + 206 m_B^2 \delta^2 + 172 m_B^3 \delta + 68 m_B^4) \\
& - 4 \log \left(\frac{\delta+m_B}{m_\phi}\right) (27 \delta^6 + 174 m_B \delta^5 + 124 m_B^3 \delta^3 + 240 m_B^5 \delta + 60 m_B^6) \left. \right] m_\phi^4 \\
& - 2 \left[(27 \delta^6 + 174 m_B \delta^5 + 454 m_B^2 \delta^4 + 612 m_B^3 \delta^3 + 422 m_B^4 \delta^2 + 110 m_B^5 \delta - 6 m_B^6) m_B^2 \right. \\
& + \coth^{-1} \left(\frac{\delta^2 + 2 m_B \delta + m_\phi^2}{\sqrt{(\delta^2 - m_\phi^2)((\delta+2m_B)^2 - m_\phi^2)}} \right) \sqrt{(\delta^2 - m_\phi^2)((\delta+2m_B)^2 - m_\phi^2)} (\delta+2m_B) \\
& \cdot (27 \delta^5 + 120 m_B \delta^4 + 214 m_B^2 \delta^3 + 172 m_B^3 \delta^2 + 50 m_B^4 \delta + 8 m_B^5) \\
& + 4 \log \left(\frac{1}{\mu^2}\right) (11 m_B^8 + 41 \delta m_B^7 + 9 \delta^3 m_B^5) + 20 \log(\delta+m_B) (2 m_B^8 + 2 \delta m_B^7 - 85 \delta^3 m_B^5) \\
& + 4 \left(-\log \left(\frac{\delta+m_B}{m_\phi}\right) m_B^2 (271 \delta^2 + 257 m_B \delta + 620 m_B^2) \delta^4 \right. \\
& + \left(36 \log \left(\frac{m_\phi^2}{\mu^2}\right) m_B^6 + \log \left(\frac{m_\phi}{\delta+m_B}\right) (9 \delta^6 + 76 m_B \delta^5 + 274 m_B^3 \delta^3 + 135 m_B^6) \right) \delta^2 \\
& + \log(m_\phi) (12 m_B^8 + 72 \delta m_B^7 + 443 \delta^3 m_B^5) \left. \right] m_\phi^2 \\
& + \left[-20 \left(\log \left(\frac{1}{\mu^2}\right) + 2 \log(\delta+m_B) \right) (23 \delta + 4 m_B) m_B^9 \right. \\
& - 2 \delta^2 \log \left(\frac{m_\phi^2}{\mu^2}\right) (36 \delta^3 + 216 m_B \delta^2 + 484 m_B^2 \delta + 497 m_B^3) m_B^5 + 4 \delta^6 \log \left(\frac{m_\phi}{\delta+m_B}\right) (208 \delta^2 + 795 m_B^2) m_B^2 \\
& + (18 \delta^8 + 152 m_B \delta^7 + 519 m_B^2 \delta^6 + 918 m_B^3 \delta^5 + 954 m_B^4 \delta^4 + 688 m_B^5 \delta^3 + 382 m_B^6 \delta^2 + 116 m_B^7 \delta + 3 m_B^8) m_B^2 \\
& + 2 \delta \coth^{-1} \left(\frac{\delta^2 + 2 m_B \delta + m_\phi^2}{\sqrt{(\delta^2 - m_\phi^2)((\delta+2m_B)^2 - m_\phi^2)}} \right) \sqrt{(\delta^2 - m_\phi^2)((\delta+2m_B)^2 - m_\phi^2)} \\
& \cdot (\delta+2m_B)^3 (9 \delta^4 + 22 m_B \delta^3 + 24 m_B^2 \delta^2 + 20 m_B^3 \delta + 6 m_B^4) \\
& \left. \left. - 2 \delta^2 \log \left(\frac{\delta+m_B}{m_\phi}\right) (9 \delta^8 + 94 m_B \delta^7 + 1028 m_B^3 \delta^5 + 1720 m_B^5 \delta^3 + 1600 m_B^6 \delta^2 + 1480 m_B^7 \delta + 1090 m_B^8) \right] \right\}. \tag{16}
\end{aligned}$$

- [2] R. Aaij *et al.* [LHCb Collaboration], JHEP **1705**, 030 (2017) [arXiv:1701.07873 [hep-ex]].
- [3] R. Aaij *et al.* [LHCb Collaboration], Phys. Rev. Lett. **118**, 182001 (2017) [arXiv:1703.04639 [hep-ex]].
- [4] R. Aaij *et al.* [LHCb Collaboration], Phys. Rev. Lett. **119**, 112001 (2017) [arXiv:1707.01621 [hep-ex]].
- [5] H. X. Chen, W. Chen, X. Liu and S. L. Zhu, Phys. Rept. **639**, 1 (2016) [arXiv:1601.02092 [hep-ph]].
- [6] H. X. Chen, W. Chen, X. Liu, Y. R. Liu and S. L. Zhu, Rept. Prog. Phys. **80**, 076201 (2017) [arXiv:1609.08928 [hep-ph]].
- [7] F. K. Guo, C. Hanhart, U. G. Meißner, Q. Wang, Q. Zhao and B. S. Zou, Rev. Mod. Phys. **90**, 015004 (2018) [arXiv:1705.00141 [hep-ph]].
- [8] A. Esposito, A. Pilloni and A. D. Polosa, Phys. Rept. **668**, 1 (2016) [arXiv:1611.07920 [hep-ph]].
- [9] R. F. Lebed, R. E. Mitchell and E. S. Swanson, Prog. Part. Nucl. Phys. **93**, 143 (2017) [arXiv:1610.04528 [hep-ph]].
- [10] G. Eichmann, H. Sanchis-Alepuz, R. Williams, R. Alkofer and C. S. Fischer, Prog. Part. Nucl. Phys. **91**, 1 (2016) [arXiv:1606.09602 [hep-ph]].
- [11] S. L. Olsen, T. Skwarnicki and D. Ziemińska, Rev. Mod. Phys. **90**, 015003 (2018) [arXiv:1708.04012 [hep-ph]].
- [12] A. Ali, J. S. Lange and S. Stone, Prog. Part. Nucl. Phys. **97**, 123 (2017) [arXiv:1706.00610 [hep-ph]].
- [13] N. Barik and M. Das, Phys. Rev. D **28**, 2823 (1983).
- [14] B. Julia-Diaz and D. O. Riska, Nucl. Phys. A **739**, 69 (2004) [hep-ph/0401096].
- [15] S. Kumar, R. Dhir and R. C. Verma, J. Phys. G **31**, 141 (2005).
- [16] A. Faessler, T. Gutsche, M. A. Ivanov, J. G. Korner, V. E. Lyubovitskij, D. Nicmorus and K. Pumsa-ard, Phys. Rev. D **73**, 094013 (2006) [hep-ph/0602193].
- [17] B. Patel, A. K. Rai and P. C. Vinodkumar, J. Phys. G **35**, 065001 (2008) [J. Phys. Conf. Ser. **110**, 122010 (2008)] [arXiv:0710.3828 [hep-ph]].
- [18] N. Sharma, H. Dahiya, P. K. Chatley and M. Gupta, Phys. Rev. D **81**, 073001 (2010) [arXiv:1003.4338 [hep-ph]].
- [19] A. Bernotas and V. Simonis, arXiv:1209.2900 [hep-ph].
- [20] S. L. Zhu, W. Y. P. Hwang and Z. S. Yang, Phys. Rev. D **56**, 7273 (1997) [hep-ph/9708411].
- [21] G. S. Yang and H. C. Kim, Phys. Lett. B **781**, 601 (2018) [arXiv:1802.05416 [hep-ph]].
- [22] J. Y. Kim and H. C. Kim, Phys. Rev. D **97**, 114009 (2018) [arXiv:1803.04069 [hep-ph]].
- [23] G. J. Wang, L. Meng, H. S. Li, Z. W. Liu and S. L. Zhu, Phys. Rev. D **98**, 054026 (2018) [arXiv:1803.00229 [hep-ph]].
- [24] K. U. Can, G. Erkol, B. Isildak, M. Oka and T. T. Takahashi, JHEP **1405**, 125 (2014) [arXiv:1310.5915 [hep-lat]].
- [25] K. U. Can, G. Erkol, M. Oka and T. T. Takahashi, Phys. Rev. D **92**, 114515 (2015) [arXiv:1508.03048 [hep-lat]].
- [26] H. Bahtiyar, K. U. Can, G. Erkol, M. Oka and T. T. Takahashi, Phys. Lett. B **772**, 121 (2017) [arXiv:1612.05722 [hep-lat]].
- [27] H. Bahtiyar, K. U. Can, G. Erkol and M. Oka, Phys. Lett. B **747**, 281 (2015) [arXiv:1503.07361 [hep-lat]].
- [28] X.-L. Ren, L. S. Geng, J. Martin Camalich, J. Meng and H. Toki, JHEP **1212**, 073 (2012) [arXiv:1209.3641 [nucl-th]].

- [29] Y. Xiao, X. L. Ren, J. X. Lu, L. S. Geng and U. G. Meißner, Eur. Phys. J. C **78**, 489 (2018) [arXiv:1803.04251 [hep-ph]].
- [30] S. Weinberg, Physica A **96**, 327 (1979).
- [31] E. E. Jenkins and A. V. Manohar, Phys. Lett. B **255**, 558 (1991).
- [32] V. Bernard, N. Kaiser and U. G. Meissner, Int. J. Mod. Phys. E **4**, 193 (1995) [hep-ph/9501384].
- [33] T. Becher and H. Leutwyler, Eur. Phys. J. C **9**, 643 (1999) [hep-ph/9901384].
- [34] T. Fuchs, J. Gegelia, G. Japaridze and S. Scherer, Phys. Rev. D **68**, 056005 (2003) [hep-ph/0302117].
- [35] L. Geng, Front. Phys. (Beijing) **8**, 328 (2013) [arXiv:1301.6815 [nucl-th]].
- [36] L. S. Geng, J. Martin Camalich and M. J. Vicente Vacas, Phys. Rev. D **80**, 034027 (2009) [arXiv:0907.0631 [hep-ph]].
- [37] L. S. Geng, J. Martin Camalich, L. Alvarez-Ruso and M. J. Vicente Vacas, Phys. Rev. Lett. **101**, 222002 (2008) [arXiv:0805.1419 [hep-ph]].
- [38] L. S. Geng, J. Martin Camalich and M. J. Vicente Vacas, Phys. Lett. B **676**, 63 (2009) [arXiv:0903.0779 [hep-ph]].
- [39] M. Z. Liu, Y. Xiao and L. S. Geng, Phys. Rev. D **98**, 014040 (2018) [arXiv:1807.00912 [hep-ph]].
- [40] A. N. Hiller Blin, Z. F. Sun and M. J. Vicente Vacas, Phys. Rev. D **98**, 054025 (2018) [arXiv:1807.01059 [hep-ph]].
- [41] X. L. Ren, L. S. Geng and J. Meng, Phys. Rev. D **89**, 054034 (2014) [arXiv:1307.1896 [nucl-th]].
- [42] Z. F. Sun and M. J. Vicente Vacas, Phys. Rev. D **93**, 094002 (2016) [arXiv:1602.04714 [hep-ph]].
- [43] D. L. Yao, Phys. Rev. D **97**, 034012 (2018) [arXiv:1801.09462 [hep-ph]].
- [44] L. S. Geng, J. Martin Camalich and M. J. Vicente Vacas, Phys. Rev. D **79**, 094022 (2009) [arXiv:0903.4869 [hep-ph]].
- [45] L. S. Geng, K. W. Li and J. Martin Camalich, Phys. Rev. D **89**, 113007 (2014) [arXiv:1402.7133 [hep-ph]].
- [46] T. Ledwig, J. Martin Camalich, L. S. Geng and M. J. Vicente Vacas, Phys. Rev. D **90**, 054502 (2014) [arXiv:1405.5456 [hep-ph]].
- [47] J. M. Alarcon, J. Martin Camalich and J. A. Oller, Annals Phys. **336**, 413 (2013) [arXiv:1210.4450 [hep-ph]].
- [48] Y. H. Chen, D. L. Yao and H. Q. Zheng, Phys. Rev. D **87**, 054019 (2013) [arXiv:1212.1893 [hep-ph]].
- [49] J. X. Lu, L. S. Geng, X. L. Ren and M. L. Du, arXiv:1812.03799 [nucl-th].
- [50] N. Jiang, X. L. Chen and S. L. Zhu, Phys. Rev. D **92**, 054017 (2015) [arXiv:1505.02999 [hep-ph]].
- [51] N. Jiang, X. L. Chen and S. L. Zhu, Phys. Rev. D **90**, 074011 (2014) [arXiv:1403.5404 [hep-ph]].